Supplementary Table S1. Primers used in this study

primer	**sequence (5' – 3')**
VapB30-f	GGAATTCCATATGGCGCTGAGTATCAAGCACC
VapB30-r	CCGCTCGAGTCAGGCCGGCAATCC
VapC30-f	GGAATTCCATATGATGGTGATCGACACGTCCGCG
VapC30-r	CCGCTCGAGTTAGGGCAGCGCGACCGTGGC
VapBC30-f	GGAATTCCATATGGCGCTGAGTATCAAGCAC
VapBC30-r	CCGCTCGAGTTAGGGCAGCGCGACCGT
$tRNA^{fMET}$_T7-f	TAATACGACTCACTATAGGGAGAGGTAGCCTGGCATTTACCGACG
$tRNA^{fMET}$_T7-r	ACCTCTGGGGTCATTTCCGCTG

Supplementary Table S2. Statistics for data collection and model refinement

A. Data collection			
Data set	SAD (Se peak)	Crystal form I (SeMet)	Crystal form II (Native)
X-ray wavelength (Å)	0.9791	0.9791	1.0000
Space group	$P3_121$	$P3_121$	$P3_121$
Unit cell length (Å)	a = b = 96.44	a = b = 96.31	a = b = 96.38
	c = 233.24	c = 233.03	c = 232.79
Unit cell angle (°)	α = β = 90, γ = 120	α = β = 90, γ = 120	α = β = 90, γ = 120
Resolution range (Å)	50.0–2.85 (2.90–2.85)[a]	50.0–2.70 (2.75–2.70)[a]	50.0–2.70 (2.75–2.70)[a]
Total /unique reflections	1,093,614 / 31,502	233,858 / 34,963	272,621 / 35,181
Completeness (%)	99.9 (100)[a]	98.9 (99.9)[a]	99.3 (99.0)[a]
$\langle I \rangle / \langle \sigma(I) \rangle$	83.4 (12.4)[a]	37.0 (4.7)[a]	41.0 (5.4)[a]
R_{merge}[b]	0.173 (0.531)[a]	0.087 (0.613)[a]	0.088 (0.693)[a]
$CC_{1/2}$		0.996 (0.944)[a]	0.998 (0.944)[a]
B. Model refinement			
R_{work} / R_{free}[c]		0.245 /0.281	0.207 / 0.244
No. of nonhydrogen atoms / average B-factor (Å^2)			
Protein		4,749 / 60.6	4,944 / 61.1
Water oxygen		55 / 48.3	103 / 48.3
Magnesium ion		2 / 44.6	3 / 40.1
Wilson B-factor (Å^2)		57.5	54.2
R.m.s. deviations from ideal geometry			
Bond lengths (Å) / bond angles (°)		0.010 / 1.42	0.011 / 1.21
R.m.s. Z-scores[d]			
Bond lengths / bond angles		0.500 / 0.640	0.566 / 0.571
Ramachandran plot (%)			
Favored		92.5[e]	94.0[e]
Outliers		0.0[e]	0.0[e]
Rotamer outliers (%)		2.5[e]	2.4[e]

[a] Values in parentheses refer to the highest resolution shell.

[b] $R_{merge} = \Sigma_h \Sigma_i | I(h)_i - \langle I(h) \rangle | / \Sigma_h \Sigma_i I(h)_i$, where $I(h)$ is the intensity of reflection h, Σ_h is the sum over all reflections, and Σ_i is the sum over i measurements of reflection h.

[c] $R = \Sigma | |F_{obs}| - |F_{calc}| | / \Sigma |F_{obs}|$, where R_{free} was calculated from a randomly chosen 5% of reflections, that were not used for structure refinement and R_{work} was calculated from the remaining reflections.

[d] Values obtained using REFMAC (39).

[e] Values obtained using MolProbity (41).

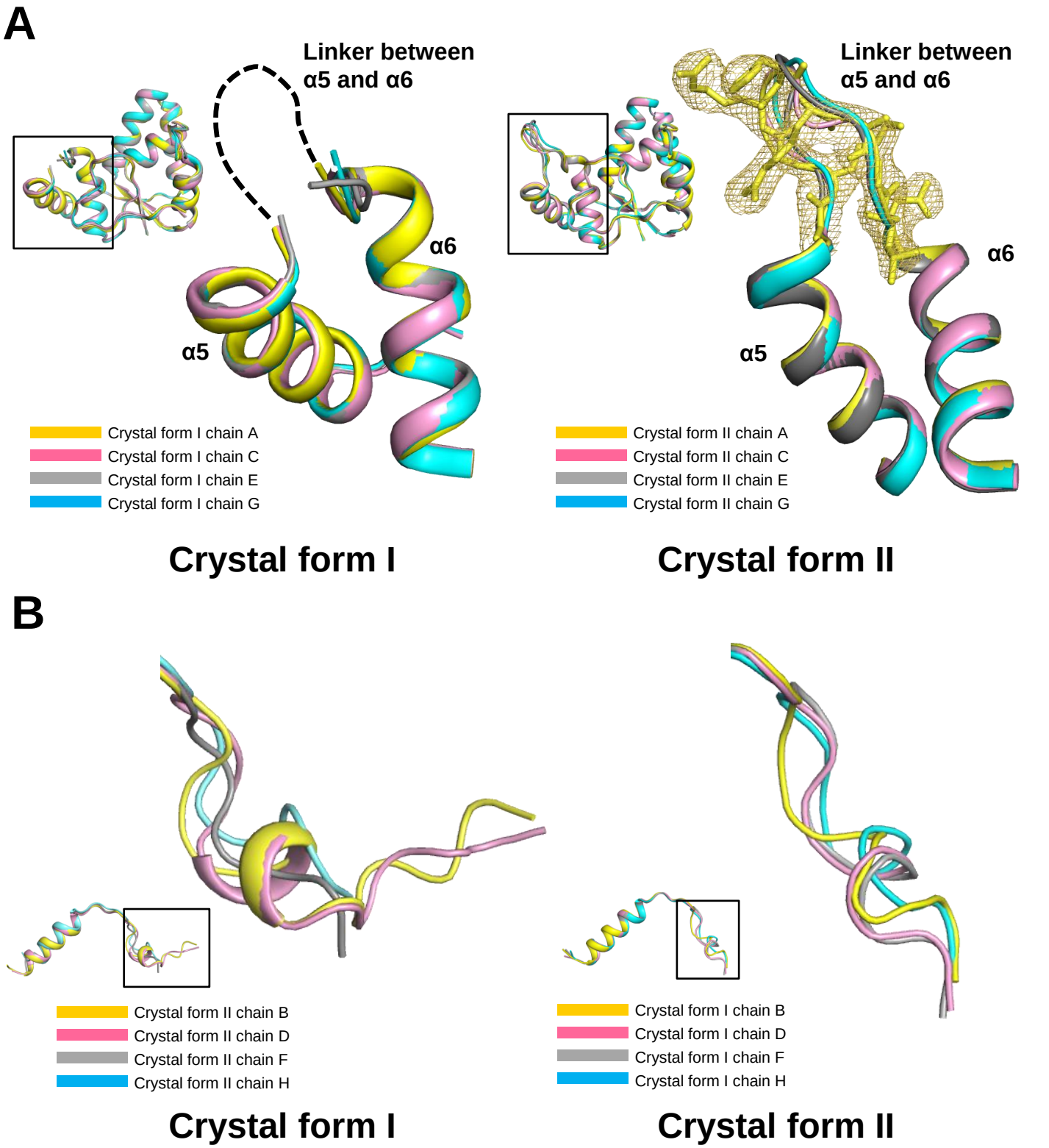

Supplementary Figure S1. Comparison of the different copies of the *M. tuberculosis* VapBC30 complex present in the asymmetric unit of crystal forms I and II. **(A)** Structural overlay of the four copies of VapC30 of crystal forms I (left) and II (right). Residues Gly89−Arg92 in the putative RNA binding loop are disordered in crystal form I, while the entire region is visible in crystal form II. Residues Gly87−Asn96 of crystal form II (chain A) are represented as stick models with its electron density map (*mFo-Fc*; contoured at 1σ, colored yellow) **(B)** Structural overlay of the four copies of VapB30 of crystal forms I (left) and II (right). The slightly different orientations and secondary structure elements in the C-terminal region of VapB30 suggest that this region is dynamic.

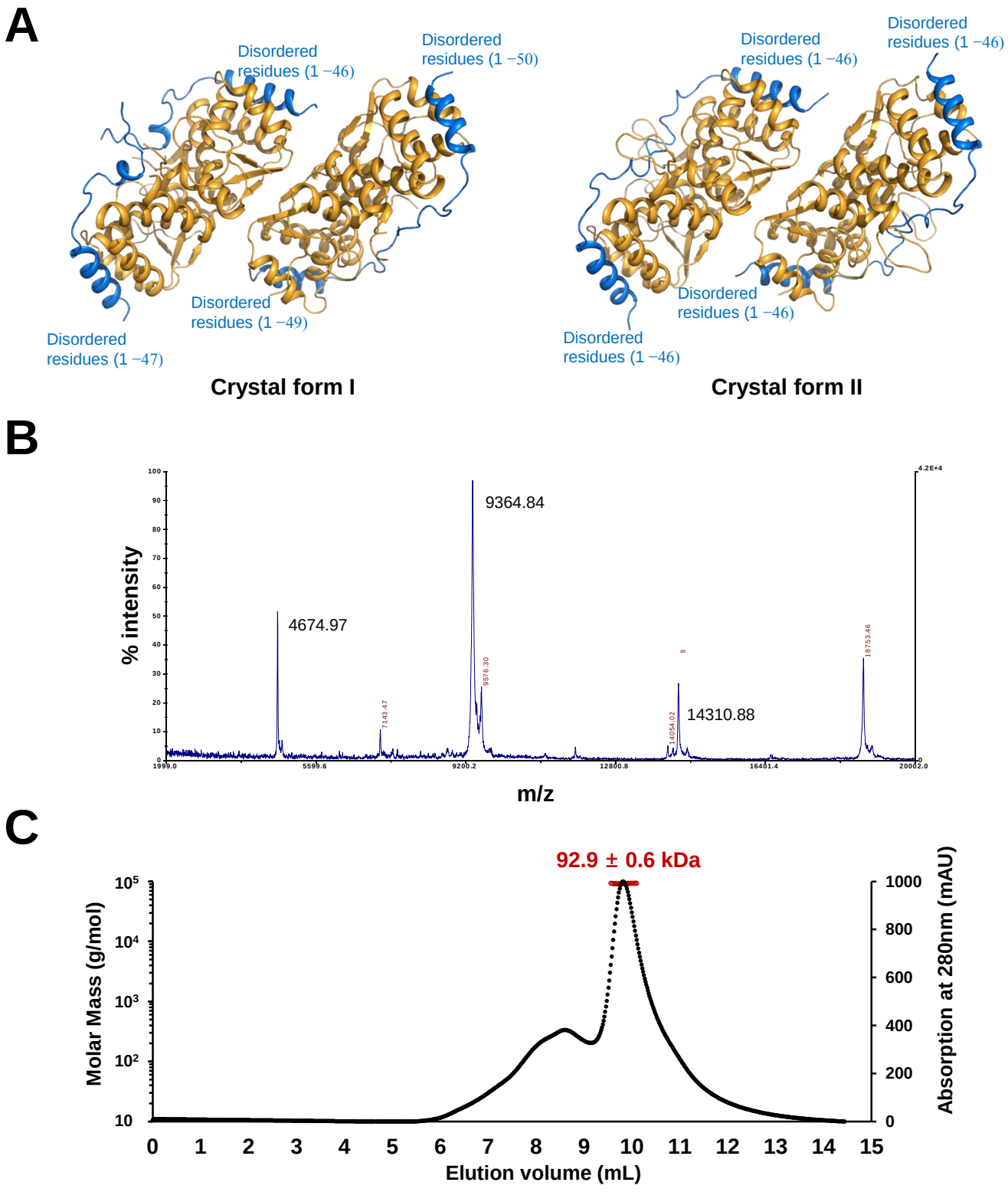

Supplementary Figure S2. *M. tuberculosis* VapBC30 exists as a heterooctamer in solution. **(A)** The crystallographic asymmetric unit of *M. tuberculosis* VapBC30 contains four copies of the VapBC30 complex in both crystal forms I (left) and II (right). *M. tuberculosis* VapC30 is shown in orange, and VapB30 is shown in blue. **(B)** MALDI-TOF spectrum of protein solution used for crystallization. **(C)** SEC-MALS chromatograms of the VapBC30 complex. The calculated molecular weight (left axis, red dotted line) and the UV absorption at 280nm (right axis, black dotted line) are plotted as a function of elution volume. Numbers above the peak indicate the average molecular weight obtained by MALS.

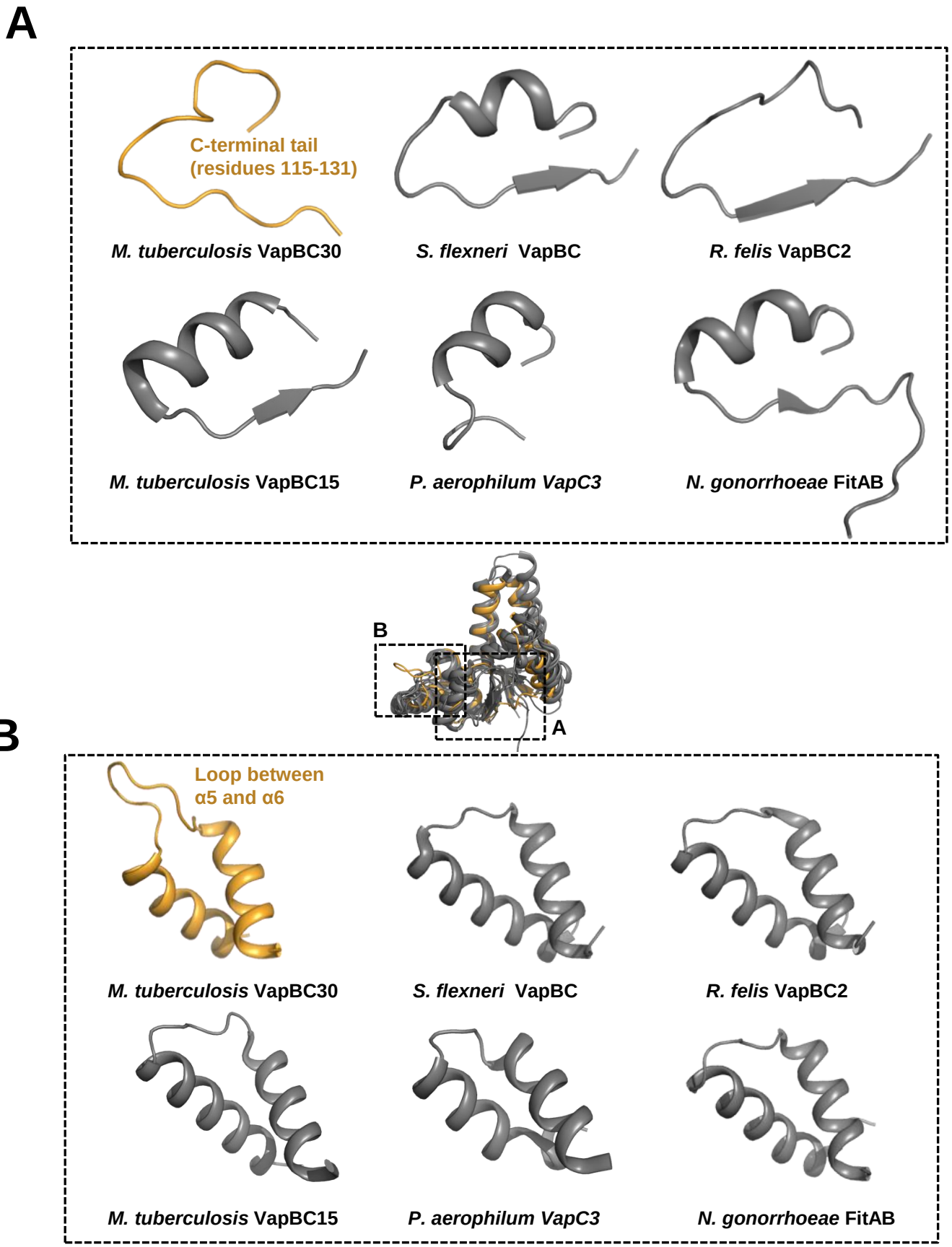

Supplementary Figure S3. Structural dissimilarities among *M. tuberculosis* VapC30 and PIN domain-containing proteins. **(A)** Comparisons of the C-terminal residues (residues 115−131) of *M. tuberculosis* VapC30 (orange) with PIN domain-containing proteins (grey). **(B)** Comparisons of the loop (residues 87−96) of *M. tuberculosis VapC30* (orange) with other PIN domain-containing proteins (grey).

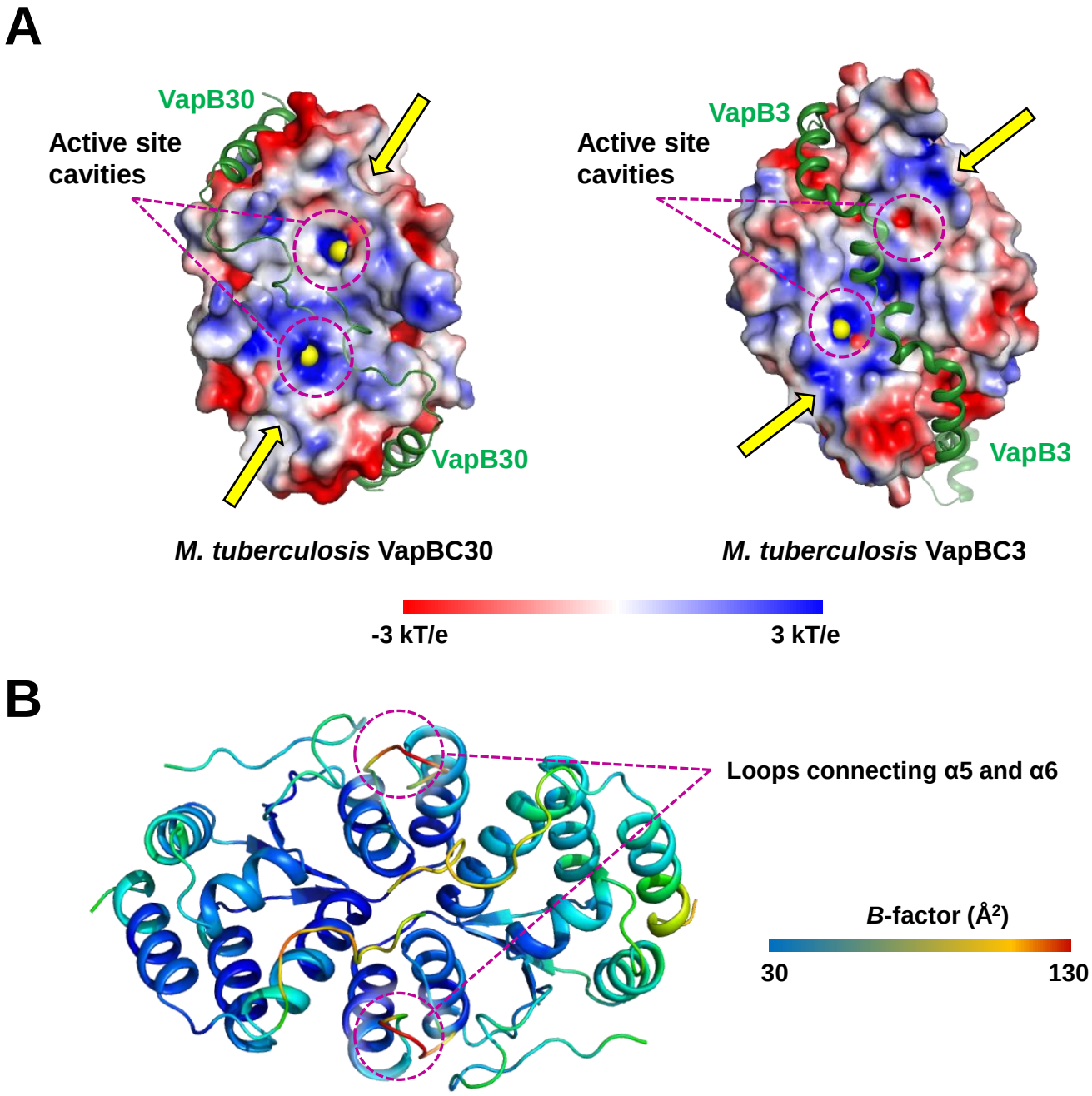

Supplementary Figure S4. Putative RNA binding loop of VapC30. **(A)** Electrostatic surface potentials of the *M. tuberculosis* VapC30 dimer of crystal form II (left) and *M. tuberculosis* VapBC3 (right), calculated with metal ions are plotted at ± 3 kT/e. The VapB30 antitoxin (left) and VapB3 antitoxin (right) are shown in cartoon representations (colored in green) and magnesium ions are shown in yellow spheres. The putative RNA binding groove and active site cavities are indicated by yellow arrows and pink dotted circles, respectively. **(B)** *B*-factor representation of *M. tuberculosis* VapC30 dimer. Note that the loops connecting α5 and α6 (pink dotted circles) have high *B*-factors, indicating a high degree of flexibility.

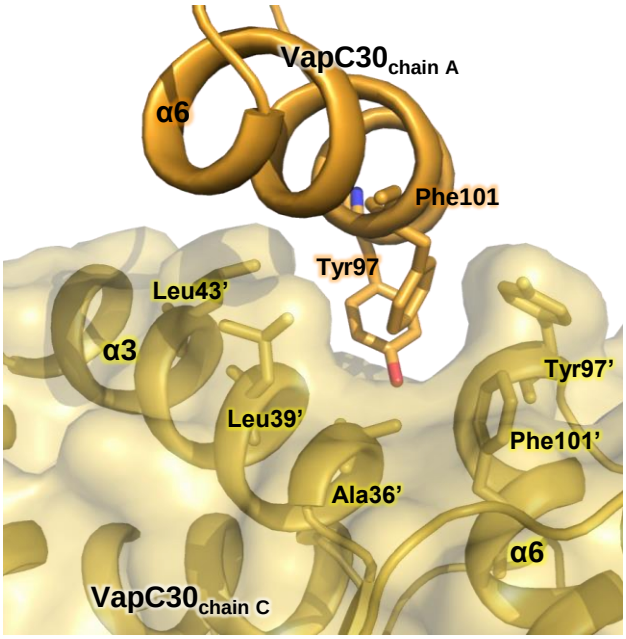

Supplementary Figure S5. Hydrophobic surface cavity formed by the hydrophobic residues Ala36, Leu39, Leu43, Tyr97, and Phe101 of VapC30 chain C. Chains A (orange) and C (yellow) are shown in cartoon representation, and chain C is shown with a partially transparent surface. For clarity, only the α6 helix of chain A and the α3, 4, and 6 helices of chain C are shown. Residues participating in hydrophobic interactions are shown in stick models.

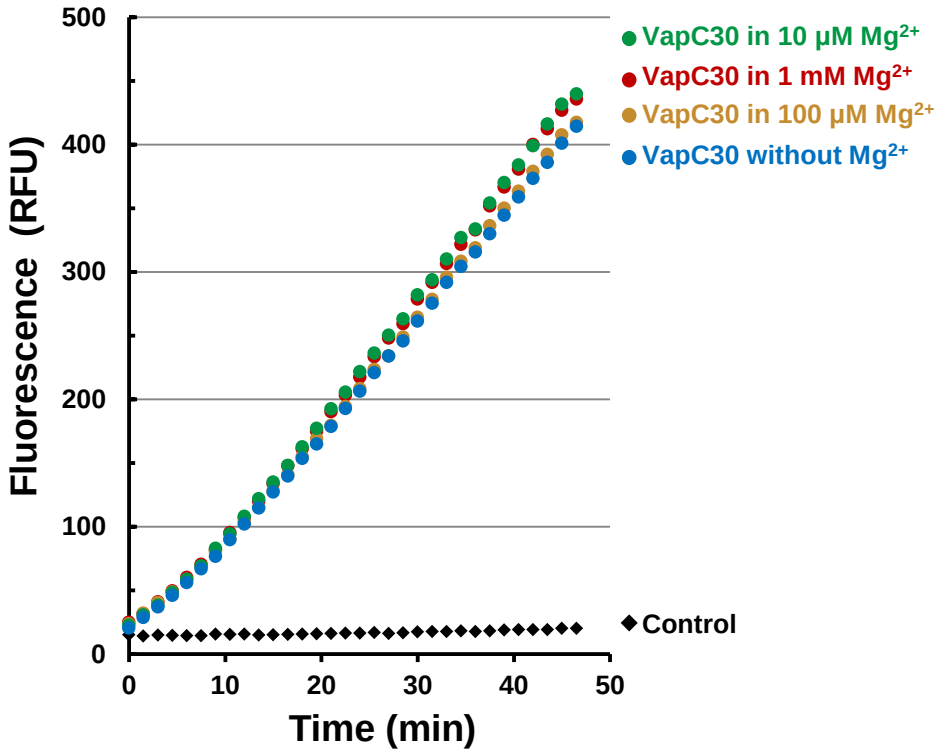

Supplementary Figure S6. Fluorescence quenching assays with 10 µM VapC30 (EDTA untreated) with various concentrations of Mg^{2+} [0 µM (blue), 10 µM (green), 100 µM (orange), and 1 mM (red)]. For the assay, 10 µM VapC30, 0.5 M NaCl, 20 mM Tris-HCl buffer at pH 8.0, 40 units of RiboLock™ RNase inhibitor (Thermo Scientific), and $MgCl_2$ were included in a 50 µl reaction volume and incubated at 37°C. Control contained 1 mM $MgCl_2$, 0.5 M NaCl, 20 mM Tris-HCl buffer pH 8.0, and 40 units of RiboLock™ (Thermo scientific) RNase inhibitor. The assay clearly demonstrated the independence of VapC30 activity on Mg^{2+} ions, when EDTA was not treated before the assay.

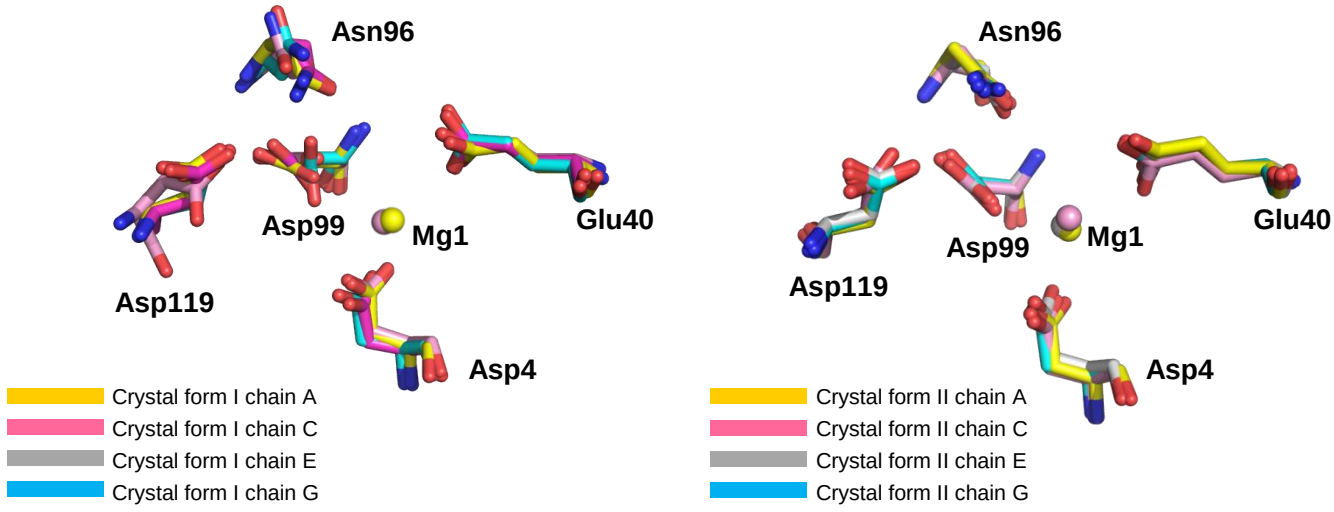

Supplementary Figure S7. Superimposition of the conserved acidic residues and Asn96 of VapC30 of crystal forms I (left) and II (right). Note the different orientations of Asn96 between chains of crystal form I. Magnesium ion (Mg1) is absent in chains E and G of crystal form I and chain G of crystal form II.

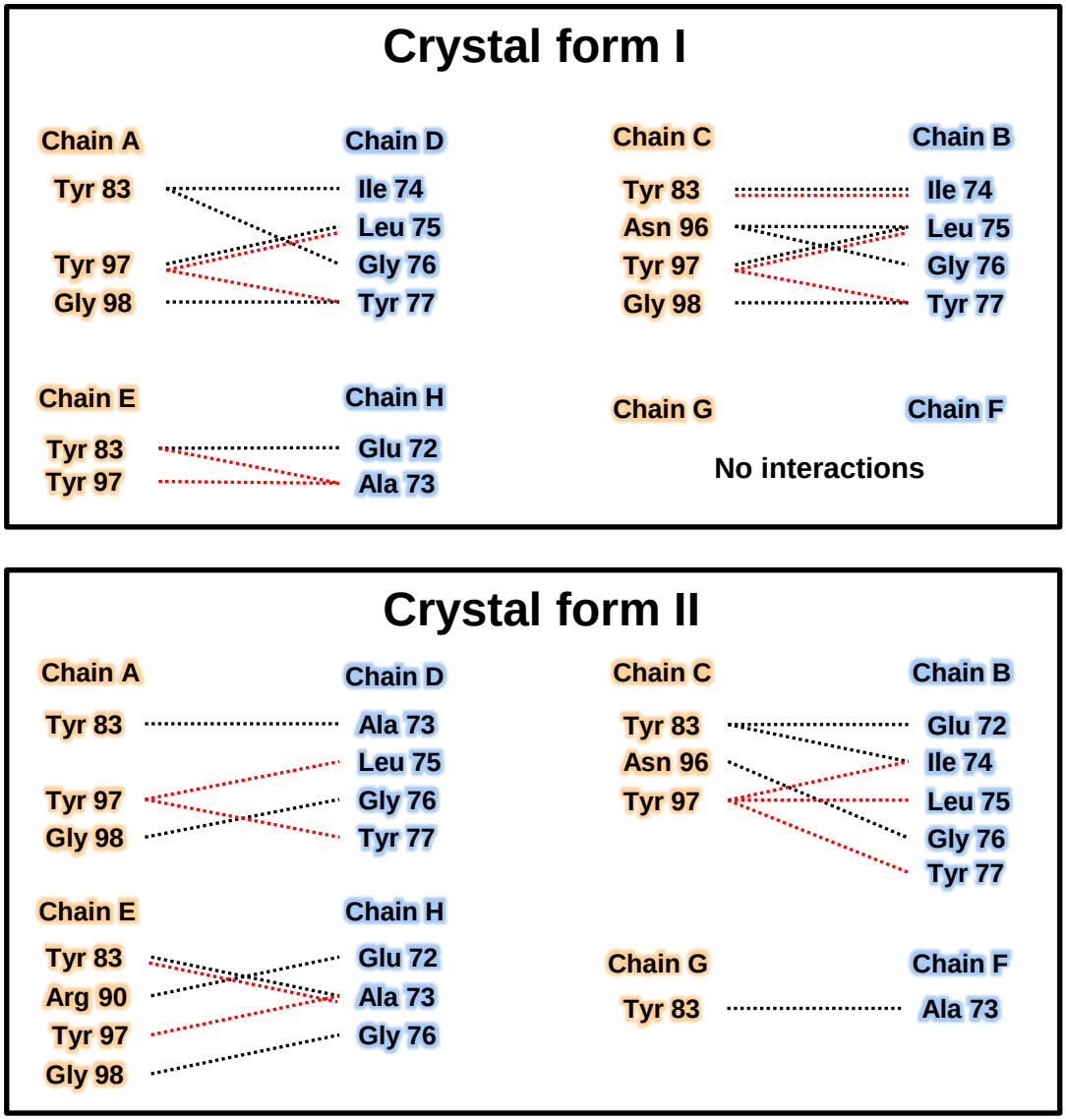

Supplementary Figure S8. Schematic diagrams of the hydrophilic interactions (black dotted lines) and hydrophobic interactions (red dotted lines) between residues of the C-terminal regions of VapB30 antitoxins and their distal VapC30 toxins. The interactions observed in crystal form I (upper) and crystal form II (lower) are shown separately.

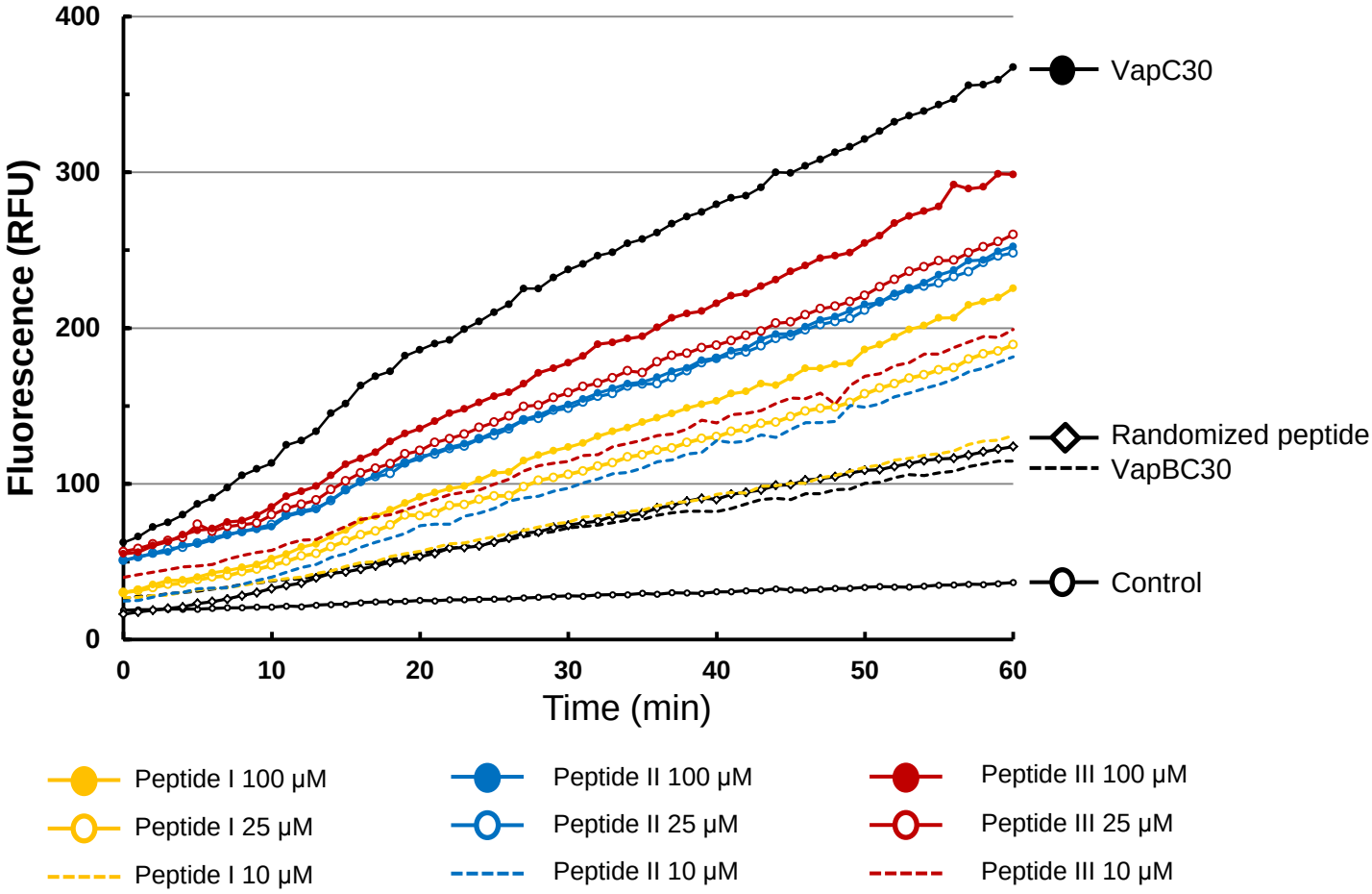

Supplementary Figure S9. Fluorescence time course experiments measuring disruption of VapBC30 complex (10 μM) by designed peptides at increasing concentrations (10−100 μM) . The negative control contained 1 mM $MgCl_2$, 0.5 M NaCl, 20 mM Tris-HCl buffer pH 8.0, 40 units of RiboLock™ (Thermo scientific) RNase inhibitor, and 100 μM of peptide I,II, and III. 100 μM of 11-mer randomized peptide (Asp-Ser-Leu-Glu-Phe-Ile-Ala-Ser-Lys-Leu-Ala) was incubated with 10 μM VapBC30 and used as control. Data shown is representative of three replicate experiments.